Solution Structure of the Supramolecular Adduct between a Liver Cytosolic Bile Acid Binding Protein and a Bile Acid-Based Gadolinium(III)-Chelate, a Potential Hepatospecific Magnetic Resonance Imaging Contrast Agent

Simona Tomaselli,[†] Serena Zanzoni,[‡] Laura Ragona,[†] Eliana Gianolio,[§] Silvio Aime,[§] Michael Assfalg,*[,‡] and Henriette Molinari[‡]

ISMAC-CNR, Via Bassini 15, 20133 Milano, Italy, Dipartimento Scientifico e Tecnologico, Università degli Studi di Verona, 37134 Verona, Italy, Dipartimento di Chimica, Università degli Studi di Torino, Via Pietro Giuria 7, Torino, Italy

Received July 7, 2008

Bile acid-conjugated gadolinium chelates were shown to display promising features for the development of hepatospecific constrast agents for magnetic resonance imaging (MRI). The study of the pharmacokinetics of these compounds should address their possible interaction with the bile acid protein transporters. We have previously shown that a 5β-cholanoic acid-based contrast agent is efficiently internalized in hepatocytes and is able to bind to a liver bile acid binding protein (BABP) in vitro. Here we report the solution structure of the adduct between a BABP and a gadolinium chelate/bile acid conjugate. The identification of unambiguous intermolecular distance restraints was possible through 3D edited/filtered NOESY-HSQC experiments, together with distance information derived from paramagnetic relaxation enhancements. These intermolecular contacts were used for the structure determination of the complex, using the data-driven docking software HADDOCK. The obtained results represent the starting point for the design of new and more efficient MRI contrast agents.

Introduction

Magnetic resonance imaging (MRI[a]) is now a commonly used diagnostic tool as it offers a powerful way to map structure and function in soft tissues by sampling the amount, flow, and environment of water protons in vivo. The intrinsic contrast can be increased by the use of contrast agents (CAs) in both clinical and experimental settings. A large part of the CAs developed earlier were composed of gadolinium(III) [Gd(III)] complexes[1,2] because of their favorable electronic and magnetic properties. In recent years, the use of gadolinium complexes of simple polyaminopolycarboxylic ligands (e.g., diethylenetriaminepentaacetic acid (DTPA) or 1,4,7,10-tetraazacyclododecane-1,4,7,10-tetraacetic acid (DOTA)) as extracellular MRI contrast agents has become more and more widespread.[3−8] At the same time, the search for complexes that are taken up by cells, particularly in the liver, has been quite active.[9−13] Gd(III) complexes in which a lipophilic residue was introduced in the basic unit of DTPA have been developed as hepatospecific agents (e.g., Gd-BOPTA,[14] Gd-EOB-DTPA[15]). Compared to the extracellular contrast agents, these "lipophilic" complexes are taken up to a variable extent by hepatocytes in different animal species and in humans,[16] although they appear to be internalized by a passive diffusion process.[17]

More recently, the interest has grown in CAs that enter the cells by means of active transport mechanisms. A variety of contrast agents have been developed for contrast-enhanced MRI of the liver, which are designed to overcome the limitations of unspecific tissue uptake by extracellular low molecular weight gadolinium chelates.[18] Active molecular transport in hepatocytes may be conveniently realized by exploiting the enterohepatic circulation machinery. The latter is an efficient recycling mechanism by which bile salts, which are synthesized in the liver from cholesterol, enter the intestine in the form of bile, where they are absorbed by the enterocytes and transferred back to the liver through the portal vein. The key steps at both the hepatocytes and the enterocytes are mediated by a receptor system, an intracellular protein carrier, and an exit system.[19] On the basis of the knowledge of bile salt transport, a number of potential CAs were synthesized by conjugating bile acid moieties to gadolinium chelating units such as DTPA or DOTA and tested in terms of pharmacokinetic properties and toxicology.[6] Among the most promising compounds, a conjugate in which the Gd(III) complex is linked to cholic acid through the 3α hydroxyl group seems to enter hepatocytes using the Na^+/taurocholate transporter. Because it has been shown that the Na^+/taurocholate transporter is not expressed in the basolateral membrane of some human hepatoma cell lines,[20] the discovery of a contrast agent that is transported into hepatocytes by such a transporter could, in principle, allow clear-cut diagnoses of specific hepatic diseases (e.g., hepatocellular carcinoma). Noticeably, two related Gd-DTPA-based conjugates of cholanoic (Gd-1) and deoxycholic (Gd-2) acid (Scheme 1) were shown to display differential cellular uptake between human healthy model cells and hepatoma cell lines.[21]

The study of the mechanisms involved in the transport of the compound by the hepatocytes is crucial for the definition of the drug's pharmacokinetics as well as to explain the relaxivity properties that are at the basis of the magnetic resonance imaging technique. While a few studies have ad-

* To whom correspondence should be addressed. Phone +39 0458027949. Fax +39 0458027929. E-mail: michael.assfalg@univr.it.

[†] ISMAC-CNR.

[‡] Dipartimento Scientifico e Tecnologico, Università degli Studi di Verona.

[§] Dipartimento di Chimica, Università degli Studi di Torino.

[a] Abbreviations: MRI, magnetic resonance imaging; CA, contrast agent; DTPA, diethylenetriaminepentaacetic acid; DOTA, 1,4,7,10-tetraazacyclododecane-1,4,7,10-tetraacetic acid; BABP, bile acid binding proteins; cl-BABP, chicken liver bile acid binding proteins; CHA, cholic acid; CDA, chenodeoxycholic acid; NOESY, nuclear Overhauser effect spectroscopy; HSQC, heteronuclear single quantum coherence; NOE, nuclear Overhauser effect; rmsd, root-mean-square deviation; AIR, ambiguous interaction restraint; CSP, chemical shift perturbation.

10.1021/jm800820b CCC: $40.75
Published on Web 10/22/2008

Scheme 1. Structure of the Gd-1, Gd-2, and Y-1 Ligands

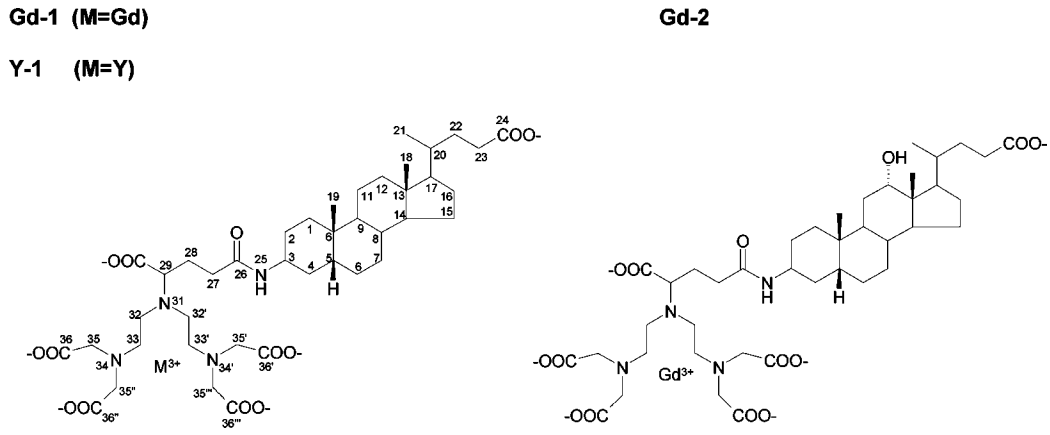

dressed the cellular uptake and excretion of bile salt-CAs, as outlined above, little is known about the mechanisms of intracellular transport. Small proteins belonging to the family of the intracellular lipid binding proteins are found to be the major bile salt carriers both in the liver and the ileum[22] and are called bile acid binding proteins (BABPs). It is therefore legitimate to consider that bile acid-based molecules such as the above-described CAs may interact with these transporters inside the cell. Chicken liver BABP (cl-BABP) is the most characterized liver BABP. Crystallographic[23] and NMR[24] studies described its fold in terms of a β-clam structure with a two-helical lid and established its ability to bind two bile salt molecules. NMR dynamic and interaction studies further pointed out the relevant role of protein mobility in ligand binding and probable allosteric regulation.[25,26]

Recently, we have reported on the in vitro interaction between a number of related CAs and chicken liver BABP.[21] By use of relaxometric measurements and high resolution NMR, we observed that the protein is able to bind a single ligand molecule with a significantly low dissociation constant, down to 20 μM as observed for compound Gd-1, despite the presence of the non-native bulky chelate moiety linked to the bile acid scaffold. These results prompted us to study the structural details of the above protein−drug interaction to set the basis for the rational design of more efficient hepatospecific CAs. We describe here the NMR solution costructure of chicken liver BABP and compound Gd-1 (cl-BABP/Gd-1), determined by using both paramagnetic structural restraints as well as intra- and intermolecular restraints obtained from experiments on a diamagnetic analogue of the Gd-1 compound. This structure represents the first structure of a BABP with a synthetic drug and is here compared to known complexes with putative native ligands.

Results and Discussion

Protein Resonance Assignments and Protein Fold Determination of Holo cl-BABP. Because the strong paramagnetism of Gd-1 quenches or attenuates all atom resonances in its spatial proximity, NMR experiments for protein resonances assignment were done using the diamagnetic analog Y-1 (Scheme 1), where the gadolinium ion is substituted by an yttrium ion. The two cations are isoelectronic, they have the same charge (+3) and very similar ionic radii (1.053 Å, Gd^{3+} and 1.019 Å, Y^{3+}).[27] It was further observed that chelating compounds such as DOTA and DTPA coordinate the two ions with the same tricapped trigonal prism coordination geometry.[28−30] This substitution is therefore not expected to introduce significant perturbations in the molecular structure and solution dynamics of the complex. The resonance assignment of signals from backbone and side chains atoms of holo cl-BABP was performed as described in the Experimental Section, using standard 3D heteronuclear multidimensional NMR experiments based on through-bond scalar connectivities[31] recorded on a sample of ^{15}N and ^{13}C labeled protein in complex with unlabeled Y-1. The assignment is complete except for amide resonances of M73, N86, K95, and E99, which could not be univocally assigned due to signal overlap. Assignment tables have been deposited in the BioMagResBank.

The secondary structure elements of holo cl-BABP, as derived from chemical shift data with the software TALOS, include 10 antiparallel β-strands and two α-helices. The strands comprise residues 5−12 (strand A), 37−42 (B), 46−53 (C), 57−63 (D), 68−72 (E), 76−85 (F), 88−93 (G), 95−103 (H), 105−112 (I), and 116−123 (J). The α-helices are composed of residues 14−21 (H1) and 26−32 (H2).

The success of docking procedures for the structural determination of protein−ligand complexes is related to the availability of accurate starting protein tertiary structures. Particularly, when the protein undergoes substantial structural rearrangement upon ligand binding, significant improvement of the final complex structure is achieved if the structure of the holo protein is used instead of the one corresponding to the apoprotein. The structures of cl-BABP in complex with cholic acid (CHA) and chenodeoxycholic acid (CDA) were determined previously by X-ray crystallography[23] and NMR spectroscopy,[24] respectively, and appeared to be very similar to each other. However, the structure of BABP when bound to Gd-1 could not be expected to be the same as the above structures, as inferred from the different HSQC spectra of the respective protein complexes. Therefore, the starting "holo" structure for the successive docking calculation was de novo determined. Intramolecular restraints used to determine the protein fold included dihedral angles derived from TALOS and interproton distances obtained from a NOESY-[^1H,^{15}N]-HSQC spectrum as well as NOESY-[^1H,^{13}C]-HSQC spectra optimized for the aliphatic or the aromatic side chains. Structural calculations were performed using CYANA 2.1,[32] implementing an efficient protocol for structure calculation/automated NOE assignment. The 20 structures with the lowest target function were selected to represent the NMR solution structure of the holo protein. The structures were determined with very high precision, as evident from the rmsd values of 0.52 ± 0.12 Å for the backbone, and 1.19 ± 0.10 Å for all heavy atoms. The quality of the structures appeared very good, with 98% of the residues occupying the

Table 1. Statistics for the Final Structural Ensemble Obtained for the Complex BABP/Gd-1

average rmsd (Å)	
⟨rmsd⟩ backbone (C_α, N^H, and C′)[a]	0.52 ± 0.12
⟨rmsd⟩ heavy atoms	1.19 ± 0.10
experimental restraints	
intraresidue NOEs	491
sequential NOEs ($\|i - j\| = 1$)	583
medium-range NOEs ($1 \leq \|i - j\| \leq 4$)	346
long-range NOEs ($\|i - j\| \geq 5$)	767
total number of distance restraints	2187
manually assigned NOEs	150
TALOS dihedral angle restraints	176
experimental restraints violations	
distances with violations[b] > 0.3 Å	3
distances with violations[b] > 0.5 Å	2
dihedral angles with violations[c] > 5°	18
Ramachandran plot (%)	
residues in most favored regions	98
residues in generously allowed regions	1.1
residues in disallowed regions	0.9

[a] Root mean square deviations of atomic coordinates were calculated over residues 1−125 using MOLMOL. [b] Distance restraint violations observed in at least one of the 20 structures. [c] Dihedral angle violations observed in at least one of the 20 structures.

most favored regions of the Ramachandran torsion angle space. The overall statistics for the final structural ensemble is reported in Table 1.

Ligand Resonance Assignment and Experimental Intermolecular Structural Restraints. The stoichiometry of binding of Gd-1 to cl-BABP was established in our previous work as 1:1 based on high resolution NMR as well as relaxometric analyses.[21] The structure determination of the complex was based on the structure obtained for the holo protein as well as the introduction of intermolecular restraints in structural calculations. The chosen structure determination procedure allows for the introduction of ambiguous interaction restraints (AIRs). The latter were obtained from chemical shift perturbations (CSPs) and paramagnetic-induced intensity attenuations of protein amide resonances observed upon ligand binding and measured in a previous work.[21] These experiments did not require ligand resonances assignments. The identified interacting residues were defined as active according to the software's definition, while the adjacent residues were defined as passive (Table 2).

For the observation of unambiguous intermolecular contacts, we analyzed samples composed of a $^{15}N,^{13}C$-labeled protein bound with unlabeled ligand and used editing and filtering techniques to identify the resonances from the two molecular species. Most NMR experiments for the determination of intermolecular restraints were recorded using the diamagnetic analogue Y-1. A 4-fold excess of ligand was used in the experiments because of a measured dissociation constant of about 20 μM and because, from the inspection of the titration curves, the protein backbone amide chemical shift perturbations produced by ligand binding appear to reach a plateau at a protein:ligand ratio of about 1:4. The identification of intermolecular distance restraints was made difficult by the intrinsically poor chemical shift dispersion of protons belonging to the steroid moiety of Y-1, as well as the complex second-order spectra of the metal ion chelating unit. However, the methyl resonances of the steroid moiety, C18, C19, and C21, appear as high-intensity signals at relatively high fields and represented a good

Table 2. Active and Passive Residues of cl-BABP Used to Define the Ambiguous Interaction Restraints within HADDOCK (in Parenthesis Are the Experimental Methods Used to Define the Residue as Active)

active	passive
A10 (CSP[a])	Y9, Q11
E15 (CSP)	Y14, E16
L23* (CSP, attenuation[b], NOE[c])	A22
E25 (attenuation)	P24
D26 (CSP, attenuation)	L27
D33 (attenuation)	R32
T53 (attenuation)	K52
R55 (attenuation)	P54
T57 (attenuation)	V58
T72 (attenuation)	T71
M73 (NOE)	
D74* (NOE)	
G75* (attenuation)	K76

[a] CSP: chemical shift perturbation. [b] Attenuation: signal intensity attenuation in the presence of the paramagnetic ligand. [c] NOE = filtered NOESY data. [d] residues used both as ambiguous and unambiguous restraints.

entry point for the assignment of the bound molecule. Indeed, the methyl resonances from both the free and bound molecules, displaying slow chemical exchange compared to the NMR time scale, are identified from the 2D F_2-[$^{15}N,^{13}C$]-filtered-[$^1H,^1H$]-NOESY spectrum (Figure 1A). Exchange peaks in the spectrum allowed us to unambiguously assign the methyl resonances of the bound molecules starting from the known assignments of the free ligand. The above cross-peaks were confirmed as exchange peaks by running a series of ROESY spectra with varying mixing times because they always displayed the same sign as the diagonal (Figure 1B). In addition to the methyl groups, other unambiguously assigned resonances corresponded to H1, H2, H3, and H4 of the first steroid ring, and to H27, H28, and H29 of the linker between the steroid ring A and the chelating moiety (see Scheme 1 for numbering).

Despite the nonoptimal binding affinity, several intermolecular NOEs were observed in a 3D F_1-[^{13}C]-filtered, F_2-[^{13}C]-separated, F_3-[^{13}C]-edited NOESY-HSQC spectrum. Fourteen intermolecular NOEs were assigned (listed in Table 3), and some of them are shown in Figure 2. They were subsequently used as unambiguous interaction restraints in the complex structure calculation. However, because the filtered experiments do not provide signals corresponding to known distances, no calibration of the peak volumes was performed, and an upper limit distance of 6 Å was introduced. A single intermolecular distance, namely that between A22-Hβ and Y-1-H27, could be obtained directly from cross-peak volume analysis of a NOESY-[$^1H,^{13}C$]-HSQC spectrum after calibration based on known intramolecular distances.

While observation and assignment of intermolecular NOEs allowed us to derive distance restraints between the protein and the steroid moiety of the ligand, no information was obtained from these experiments concerning the metal ion chelating group. Still, it is important to get knowledge about the relative position of this unit that is separated from the steroid scaffold by five rotatable torsion angles. Information derived from paramagnetic centers has long been introduced into structure calculations of metalloproteins, proteins modified to introduce metal chelates or radicals, as well as protein−protein complexes.[33,34] Indeed, paramagnetic centers produce perturbations of protein signals which are distance-dependent and can be of long-range effect.[35] Gadolinium(III) complexes are highly paramagnetic because of the presence of seven unpaired electrons. The high spin multiplicity is maintained also after complexation by common chelating agents,[36,37] and the spherical symmetry of the 4f orbitals explains the absence of chemical shift effects on

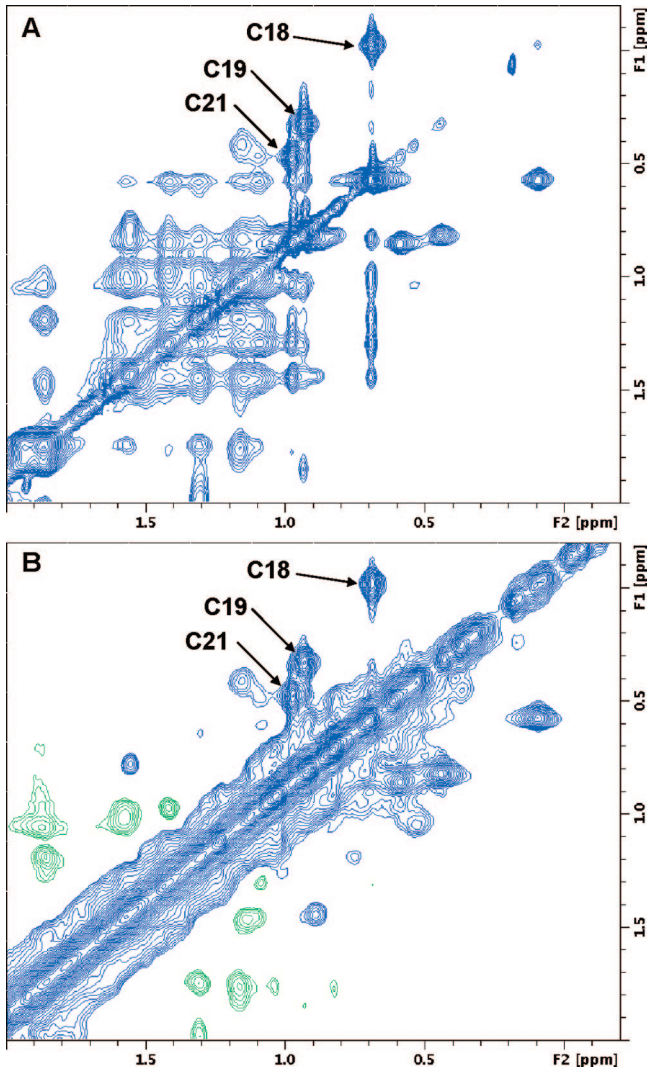

Figure 1. (A) High field region of an F_2-[^{15}N,^{13}C]-filtered-[^{1}H,^{1}H]-NOESY spectrum recorded at 600 MHz, 25 °C, pH 7.0 with 80 ms mixing time. The sample was a [^{15}N/^{13}C] cl-BABP in the presence of a 4-fold excess of [*u*]Y-1. (B) Same region of a [^{1}H,^{1}H]-ROESY experiment recorded in the same conditions as above, with a spin-lock time of 50 ms. Marked peaks are exchange peaks between the proton methyl signals of the free and the bound ligand corresponding to methyl positions C18, C19, and C21.

the signals of nearby nuclei. On the other hand, unpaired electrons markedly affect the nuclear relaxation of neighboring nuclei through dipolar mechanisms. The paramagnetic enhancement of longitudinal relaxation rates of amide protons, R_{1p}, is proportional to the inverse of the sixth power of the metal−proton distance and can thus be exploited to derive structural restraints to place the metal center in the correct position with respect to the protein, once an estimate of the proportionality constant is given. R_{1p} values were here calculated as the difference in R_1 observed between a paramagnetic and a diamagnetic protein−ligand adduct. To avoid excessive reduction in signal/noise due to the strong paramagnetism of gadolinium, the paramagnetic adduct was obtained by dilution of Gd-1 with diamagnetic Y-1. In other words, while keeping a 4-fold excess of total ligand with respect to the protein, 10% of the ligand was Gd-1 while 90% was Y-1. The relaxation rates were measured on amide protons using an inversion recovery scheme coupled to ^{15}N-editing (see Experimental Section for details).[38] Selected signal decays are shown as an example in Figure 3A. The determined R_{1p} rates are plotted as a function of the residue number in Figure 3B and mapped on the protein structure in Figure 3C. Missing values are due to problems of signal overlap or low sensitivity. R_{1p} values up to 2.68 s^{-1} were determined and converted into distances (Table 3). Prior to the rate-to-distance conversion an occupancy factor of 0.1 was introduced (eq 1, Experimental Section), taking into account the reduced paramagnetic effect on protein resonances obtained after 10-fold dilution of Gd-1 by the diamagnetic Y-1. Because the data are redundant, in order to avoid overfitting, only the distances obtained with the lowest errors were retained and introduced into structure calculations (Table 3).

Table 3. Intermolecular Unambiguous Distance Restraints Used to Calculate the Structure of cl-BABP/Gd-1

protein atom	ligand atom	experiment	R_{1p} (s^{-1})[a]	Distance (Å)[b]
L18 Hδ	H-(C18)	NOE[c]		<6.0
L18 Hδ	H-(C21)	NOE		<6.0
K19 H_N	Gd[d]	relaxation[e]	0.47 ± 0.13	15.6
A20 H_N	Gd	relaxation	0.79 ± 0.12	14.4
L21 Hδ	H-(C19)	NOE		<6.0
L21 H_N	Gd	relaxation	1.30 ± 0.22	13.2
A22 Hβ	H-(C3)	NOE		<6.0
A22 H_N	Gd	relaxation	2.07 ± 17	12.2
A22 Hβ	H-(C40)	NOE		<6.0
L23 H_N	Gd	relaxation	1.63 ± 0.19	12.7
L27 Hδ	H-(C40)	NOE		<6.0
L27 Hβ	H-(C19)	NOE		<6.0
L27 H_N	Gd	relaxation	1.65 ± 0.36	12.7
I28 H_N	Gd	relaxation	0.89 ± 0.14	14.1
K29 H_N	Gd	relaxation	0.72 ± 0.15	14.6
M30 Hε	H-(C40)	NOE		<6.0
M30 Hε	H-(C19)	NOE		<6.0
M30 Hβ	H-(C19)	NOE		<6.0
M30 Hγ	H-(C19)	NOE		<6.0
M30 H_N	Gd	relaxation	1.47 ± 0.21	13.0
A31 Hβ	H-(C19)	NOE		<6.0
A31 Hβ	H-(C18)	NOE		<6.0
A31 H_N	Gd	relaxation	0.95 ± 0.16	14.0
*R*32 H_N	Gd	relaxation	0.33 ± 0.15	16.6
I34 H_N	Gd	relaxation	0.38 ± 0.13	16.2
S51 H_N	Gd	relaxation	0.32 ± 0.16	16.8
T53 H_N	Gd	relaxation	0.63 ± 0.20	14.9
Q56 H_N	Gd	relaxation	2.68 ± 0.61	11.7
D74 H_N	Gd	relaxation	1.81 ± 0.20	12.5
G75 H_N	Gd	relaxation	2.38 ± 0.27	12.0
K76 H_N	Gd	relaxation	1.84 ± 0.44	12.5
K77 H_N	Gd	relaxation	1.70 ± 0.34	12.6
F113 Hβ	H-(C21)	NOE		<6.0

[a] R_{1p}: paramagnetic contribution to the longitudinal relaxation rate. [b] Distance restraints consisted in upper limits if derived from intermolecular NOEs, or in an allowed interval when derived from relaxation measurements (with upper and lower distance bounds set to ± 2.0 Å of the calculated distances). [c] NOE: filtered NOESY data. [d] Gd refers to the metal center. [e] Proton longitudinal relaxation rate measurements.

Structure Calculation and Analysis of the Protein−Ligand Adduct. The calculation of the tertiary structure of the adduct between cl-BABP and Gd-1 was performed with the popular data-driven docking software HADDOCK. Contrary to the most common implementation, in this work the whole set of protein intramolecular restraints were retained during the calculations. This approach, compared to standard protein structure determination methods, has proven successful in similar studies.[39] It is close to a full complex structure determination procedure and ensures highest accuracy of the protein structure in the complex while exploiting the better capability of the docking algorithm to search in the intermolecular conformational space compared to protein structure determination software. The starting structures for ligand docking were thus given by the ten structures determined as described above. An initial ligand conformation was produced on the basis of known crystal-

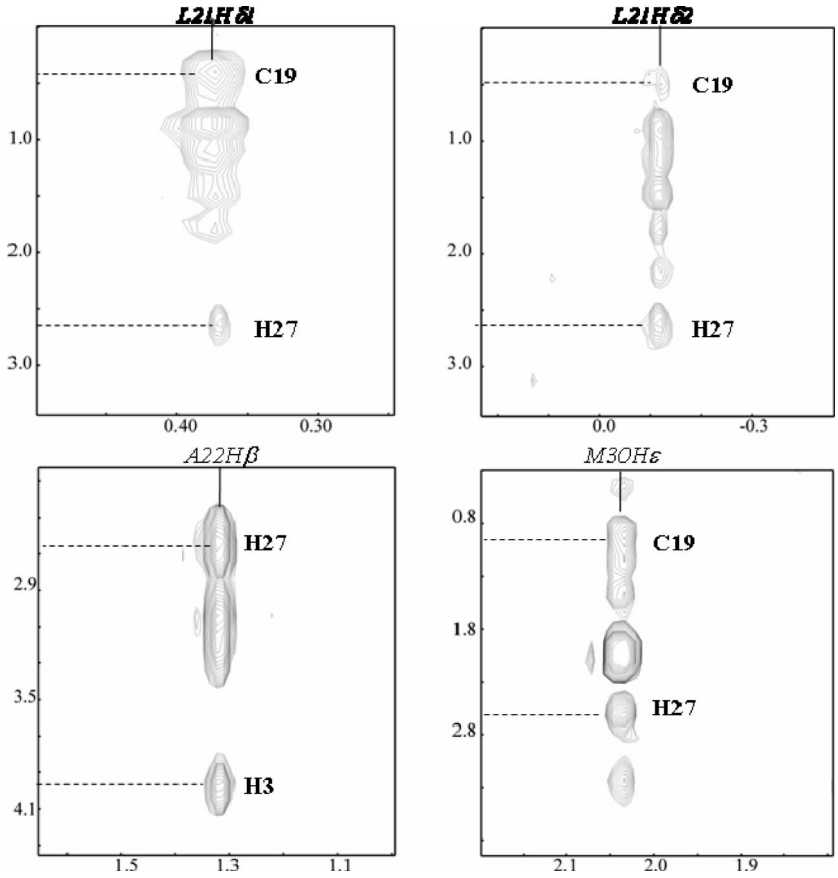

Figure 2. Selected F_1-F_3 slices of the 3D F_1-[^{13}C]-filtered, F_2-[^{13}C]-separated, F_3-[^{15}N,^{13}C]-edited NOESY-HSQC experiment showing intermolecular NOEs. The spectrum was recorded at 25 °C, 900 MHz and with 120 ms mixing time. The sample was [^{15}N/^{13}C] cl-BABP in the presence of a 4-fold excess of [*u*]Y-1, pH 7.0. Ligand resonances (bold) and protein resonances (italics) are indicated on the spectra.

lographic structures of Gd-DTPA complexes and steroid molecules.[40] HADDOCK ambiguous and unambiguous restraints employed for the calculation of the structure of the complex are reported in Tables 2 and 3, respectively. In many cases the interaction of a protein residue with the ligand was detected with more than one method: ambiguous intermolecular contacts were converted to unambiguous distance restraints if also observed in NOESY or paramagnetic relaxation enhancement experiments.

The HADDOCK structure calculation led to a final ensemble of seven structures displaying backbone and global pairwise rmsd values for protein atom coordinates of 0.66 ± 0.11 Å and 1.42 ± 0.21 Å, respectively, and an rmsd referred to ligand coordinates of 0.88 ± 0.30 Å, after superposition of all atoms. This highly consistent set of seven lowest energy structures is displayed in Figure 4. The family of structures is of good quality in terms of structural statistics and appears to largely satisfy both intramolecular and intermolecular experimentally derived restraints, as evidenced from Table 4. The proton−metal distances measured in the final docked structures (d^{dock}) are in good agreement with the experimental distances (d^{exp}) considering the value of 0.26 ± 0.01 Å assumed by the function

$$\sigma = \frac{1}{N}\sum_{i=1}^{N}\sqrt{(d_i^{\text{dock}} - d_i^{\text{exp}})^2}$$

with N corresponding to the number of distances and a correlation factor $R = 0.90 \pm 0.01$. The rmsd between the input and the docked protein coordinates is 1.06 ± 0.05 Å, with the largest differences located in helix I. The latter region, which is not very tightly restrained by intramolecular contacts, is more shifted in the direction of the ligand in the docked structure as a consequence of the introduction of six unambiguous intermolecular restraints (between residues 19, 20, 21, 22, and 23 and the metal ion) and one ambiguous restraint (residue 15).

The present structure indicates that the ligand binds to the "upper" part of the large hydrophobic protein cavity, a region called the portal area because it is thought to be the entry site for ligand binding. While the steroid moiety becomes practically buried inside the cavity, the bulky hydrophilic ion chelating moiety is completely at the exterior of the protein. It can be observed that the steroid moiety of the ligand, which is completely apolar due to the absence of hydroxyl groups that are present in bile salts, is surrounded by hydrophobic residues providing significant (25% of total) intermolecular interaction energy (Figure 5A). On the other hand, two positively charged residues, namely R120 and K76, establish polar contacts with the terminal carboxylate deep inside the protein cavity and the amide carbonyl at the opposite extreme, respectively, thereby stabilizing the observed ligand orientation. In a number of structures, another polar contact links an arginine residue, R55, to one carboxylate of the ion chelating group (Figure 5B). Table 5 reports a list of the intermolecular hydrophobic and polar interactions present in the complex.

Structural Comparisons with Known Complexes. High resolution structures of cl-BABP were previously determined,[23,24] showing the capability of the protein to bind two bile acid molecules inside a large hydrophobic cavity with high affinity. Both molecules of either cholic or chenodeoxycholic acid, which are putative native ligands, show an orientation in which ring A is buried within the protein pocket while the carboxylate group

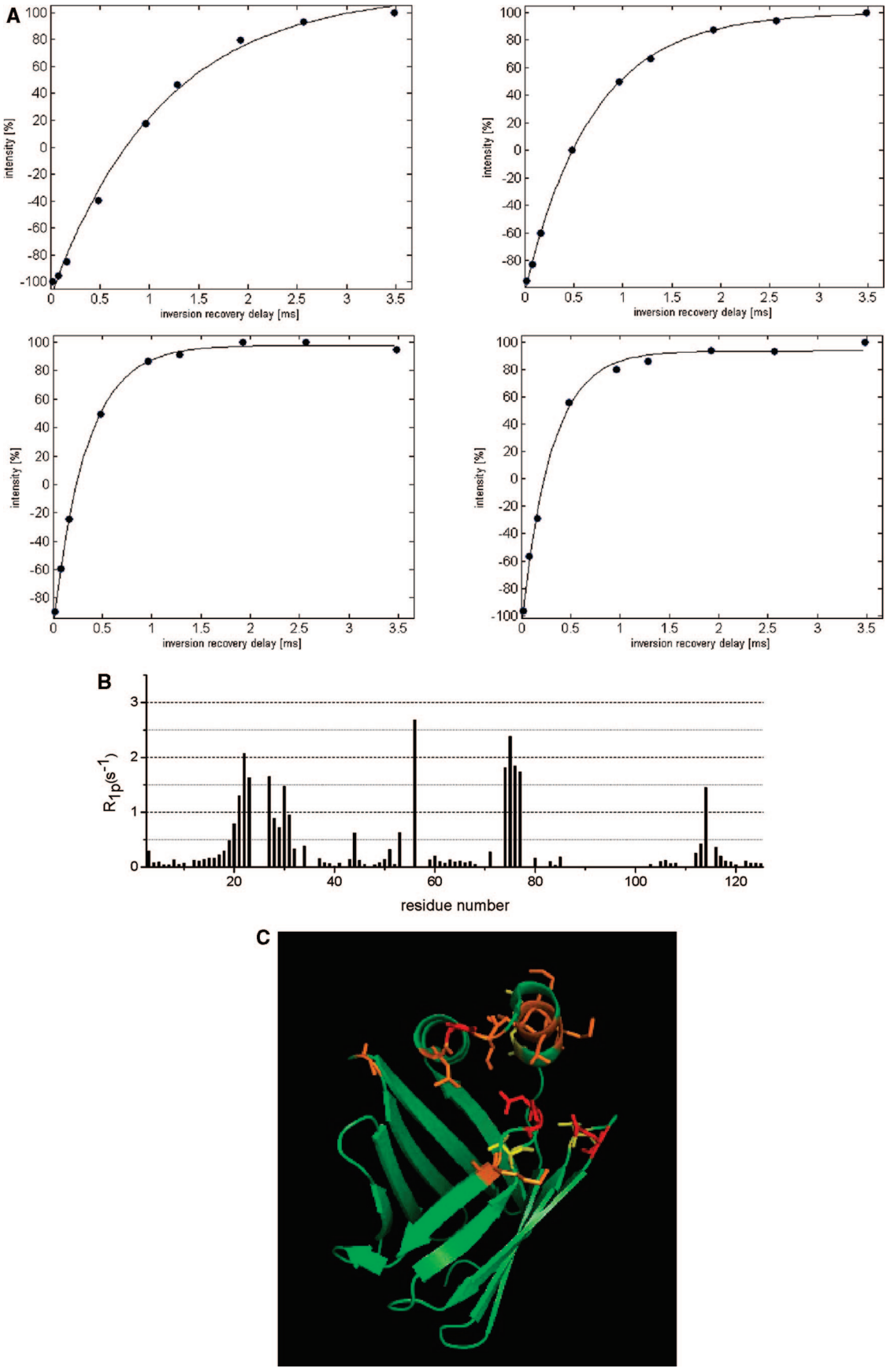

Figure 3. (A) Amide proton signal intensities as a function of increasing inversion recovery delays for residues 22 (left) and 76 (right) highlighting the different longitudinal relaxation rate in the presence of the diamagnetic (top) and paramagnetic (bottom) ligand. Fitting curves obtained with a three parameter fit of a monoexponential function are shown. (B) Paramagnetic enhancements of longitudinal proton relaxation rates as a function of the primary sequence. (C) Paramagnetic enhancements of longitudinal proton relaxation due to the presence of Gd-1 are mapped on the cl-BABP structure and color coded according to the intensity of the enhancement (red: highest attenuation).

Figure 4. Lowest-energy solution structures calculated for the complex cl-BABP/Gd-1 (PDB: 2k62). The protein in shown in ribbon representation, color coded according to secondary structure (yellow:sheet, magenta:helix). The ligand is represented in cyan sticks, while the metal ion is indicated by an orange sphere.

is fairly solvent-exposed pointing toward the helix−loop−helix motif. The latter is considered the lid that allows entrance of the ligands by its opening movement. The structure determined here differs in several respects from the above complexes. It should be noted that the bulky functionalization introduced on the ligand to carry the paramagnetic center is located at C3 of steroid moiety ring A. As a consequence, Gd-1 accesses the protein cavity in a reverse orientation with respect to bile acids, with ring A pointing toward the open end of the protein pocket (Figure 6). While the protein backbone structures of both holo CHA and CDA complexes are very similar, here we observe conformational changes in correspondence of the protein open end, which exhibits a closure of the loops surrounding the cavity entrance and an opening of the helix−turn−helix lid, which controls the access to the binding cavity. The present data confirm a stoichiometry of binding of 1:1, with Gd-1 occupying mostly the subsite that binds the more external cholic acid. The structure with CHA (1tw4) indicates that five amino acids form hydrogen bonds with the two cholate molecules, namely R55, Q56, K76, H98, and Q100. By analysis of the bundle of NMR structures with CDA (2jn3), the presence of intermolecular hydrogen bonds among the ligands and the residues R55, Q56, T72, M73, D74, K76, K95, and Q100 is found. For the cl-BABP/Gd-1 complex, intermolecular hydrogen bonds with residues R55, K76, and R120 involve the two polar tails of the ligand. The fraction of electrostatic energy contributing to the stabilization of the adducts is larger for the interaction of cl-BABP with CDA compared to Gd-1 (90% and 75% of the total interaction energy, respectively). Thus, new interactions seem to allow for an alternative medium affinity binding when reverse binding is present. Further stabilization could be achieved by appropriately introducing hydroxyl groups on the steroid moiety, considering the availability of H-bond partners along a polar spine, which was recognized as highly conserved in an earlier study on fatty acid binding proteins.[41]

Table 4. Structural Statistics of the Seven Best Structures of cl-BABP/Gd-1

average rmsd (Å)	
⟨rmsd⟩ backbone(C_α, N_H, and C′)[a]	0.66 ± 0.11
⟨rmsd⟩ heavy atoms	1.42 ± 0.21
backbone rmsd (Å) with respect to mean	
flexible interface backbone	0.44 ± 0.17
all backbone	0.48 ± 0.21
experimental restraints	
number of interaction restraints (AIRs)	
total AIRs	26
number of unambigous interaction restraints	
intermolecular restraints	33
restraints violations	
total AIR violations	2
total unambigous violations[b]	1
intermolecular energies after water refinement	
E_{vdw} (kcal mol−1)	−28.2 ± 2.7
E_{elec} (kcal mol−1)	−87.2 ± 29.9
buried surface area (Å^2)	972.4 ± 42.0
rmsd from idealized covalent geometry	
bonds (Å)	0.004 ± 0.00
angles (deg)	0.6 ± 0.02
impropers (deg)	0.55 ± 0.01
dihedrals (deg)	22.4 ± 0.5
Ramachandran plot (%)	
residues in most favored regions	98.3
residues in generously allowed regions	0.8
residues in disallowed regions	0.9

[a] Root mean square deviations of atomic coordinates were calculated over residues 1−125 using MOLMOL. [b] Distance violated in more than 30% of the structures of the final bundle.

The structural comparison of cl-BABP/Gd-1 with the other available liver BABP structures in complex with their putative ligands bears some relevance with respect to the understanding of the determinants of binding in this protein family. Few other structures of holo BABPs are presently available, all of them referring to liver proteins from nonmammalian species. We calculated and compared the positional global rmsd per residue between the cl-BABP/Gd-1 structure and the other reported holo complexes from chicken, zebrafish, and axolotl liver (Figure 7). It is clear from this comparison that the protein regions 18−29 (loop connecting the two helices and helix2), 42−46 (BC loop), 55−56 (CD loop), 84−88 (G strand), and 113−115 (IJ loop) in cl-BABP/Gd-1 display the largest structural differences to all other holo structures. This observation is consistent with the high plasticity at the level of the portal area, considered relevant for ligand binding. On the other hand, large differences are observed also in the opposite side of the cavity at the level of stretch 84−88. The latter comprises some highly conserved residues, playing a structural role in protecting the cavity from solvent. At first sight, this difference might be related to the fact that, in the cl-BABP/Gd-1 structure, the ligand does not approach the bottom of the cavity, contrary to other ternary complexes. Interestingly, however, large differences are observed with the only other singly ligated protein, namely

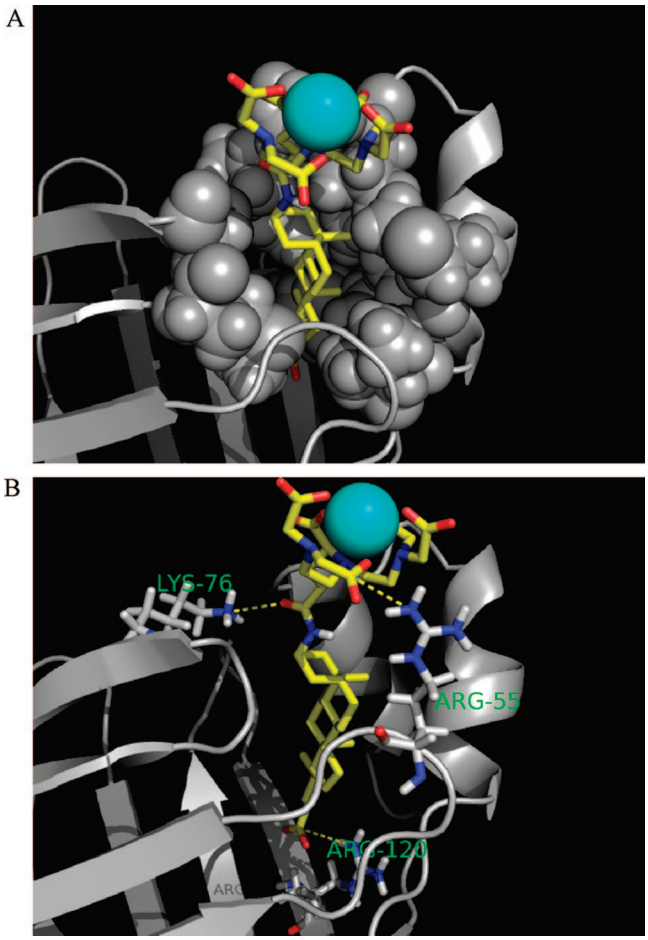

Figure 5. Hydrophobic (A) and polar (B) intermolecular contacts are highlighted on the cl-BABP/Gd-1 structure.

Table 5. Hydrophobic Interactions, H-Bonds, and Salt Bridges Present in at Least Four of the Best Seven Structures of cl-BABP/Gd-1 Calculated by HADDOCK

H-bond/salt bridges	hydrophobic interactions
K76 (F strand)	Y14 (helix I)
R120 (J strand)	F17 (helix I)
	L18 (helix I)
	L21 (helix I)
	A22 (helixI−helix II Loop)
	L23 (helix I−helix II Loop)
	M30 (helix II)
	A31 (helix II)
	L34 (helix II−B strand loop)
	M73 (EF loop)
	D74 (EF loop)
	L118 (J strand)

zebrafish liver, thus indicating that any opening motion occurring at the portal area is transmitted to the opposite side of the protein.

Conclusions

The solution structure of a liver BABP in complex with Gd-1 has been obtained using the HADDOCK procedure based on the determined NMR structure of the holo protein and both ambiguous and unambiguous intermolecular restraints derived from a variety of NMR experiments. The structure of the cl-BABP/Gd-1 complex represents the starting point for the design of new and more efficient CAs. The observations derived from structural comparison with holo proteins in complex with native ligands underline the capability of this protein scaffold to adapt

Figure 6. Structure of cl-BABP/Gd-1 (PDB: 2k62) with superimposed CDA ligands as in the ternary complex cl-BABP/CDA (PDB: 2jn3). The protein structure is shown in a green cartoon representation and the ligand Gd-1 in green sticks. The position of the CDA ligands (yellow) is obtained after global superimposition of the two complex structures.

itself to the steroid moiety, thus making this system an appropriate carrier for hepatospecific contrast agents. The analysis of the hydrogen bonding pattern in the available cl-BABP complexes suggests that a further design could take into account the introduction, on the steroid moiety, of hydroxyl groups, which play some important role in fine-tuning polar interactions with conserved polar residues, always involved in ligand binding.

Experimental Section

Protein Expression and Purification. Recombinant cl-BABP was expressed as soluble protein in *Escherichia coli* cells, purified with anion exchange and size-exclusion chromatography, and finally delipidated following already described protocols.[25] Uniform ^{15}N and ^{13}C isotope labeling was achieved using M9 minimal media containing 1 g/L $^{15}NH_4Cl$ and 4 g/L ^{13}C enriched glucose.

Ligand Synthesis. The bile acid conjugate was prepared as previously described[6] and kindly supplied by Bracco Imaging Spa (Milan).

NMR Experiments and Data Analysis. All samples were prepared in 30 mM sodium phosphate buffer, pH 7.0, containing 0.03% NaN_3 and 95%/5% H_2O/D_2O or 99%D_2O. NMR spectra were acquired at 25 °C on Bruker spectrometers Avance III 600 and Avance 900, both equipped with a 5 mm TCI cryoprobe and *Z*-field gradient. Data were processed with NMRPipe[42] and visualized by NMRView.[43]

The following experiments were run on the adduct between the [$^{15}N/^{13}C$]cl-BABP and unlabeled diamagnetic yttrium analogue [*u*]Y-1 (Scheme 1). A protein:ligand ratio of 1:4 was used with a final protein concentration of 0.5 mM. The sequential amino acid resonances assignment has been previously described,[21] and was here completed through the analysis of HNCACB, CBCA(CO)NH, HN(CA)CO, and HNCO triple resonance experiments collected at 600 MHz. Side chain carbon and proton resonances were assigned based on (H)CCH-TOCSY, H(C)CH-TOCSY, and HBHA(CO)NH spectra. The resonance assignments were submitted to the BioMagResBank under accession number 15854. Intramolecular NOE-based distance restraints were extracted from 3D NOESY-[$^1H,^{15}N$]-HSQC, NOESY-[$^1H,^{13}C$]-HSQC in H_2O, as well as NOESY-[$^1H,^{13}C$]-HSQC and NOESY-[$^1H,^{13}C$]-HSQC spectra in D_2O optimized for the aromatic side chains, all acquired at 600 MHz.

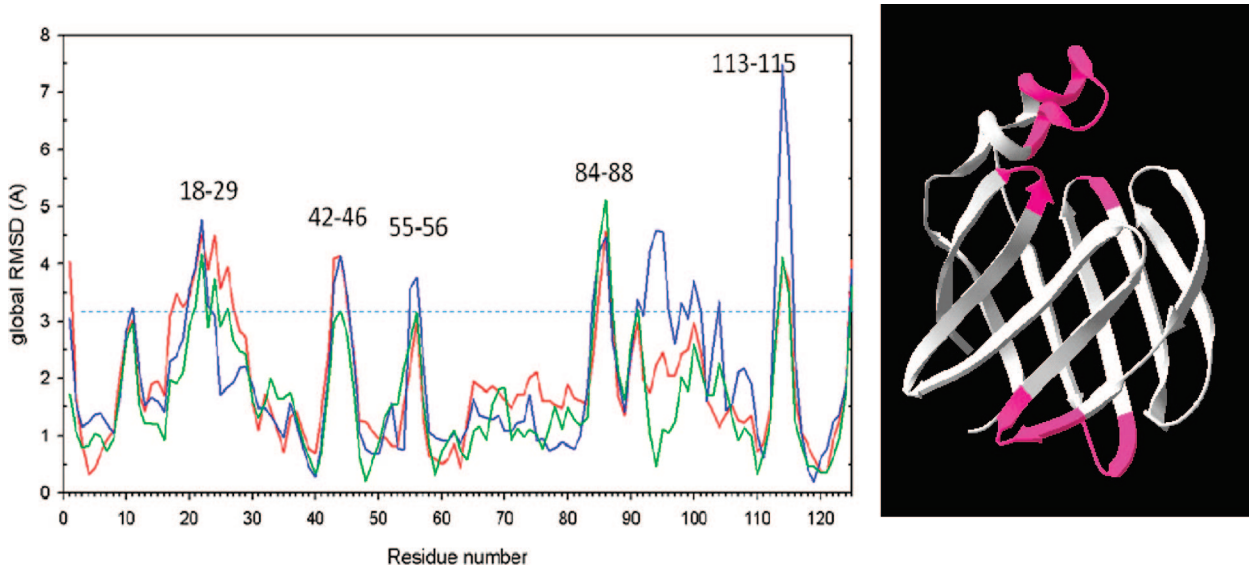

Figure 7. Left panel: average global rmsd between the backbone atoms of the cl-BABP/Gd-1 complex (PDB 2k62) and cl-BABP in complex with CDA (red, PDB 2jn3), liver zebrafish BABP/CHA (blue, PDB 2qo4), liver axolotl BABP/CHA (green PDB 2ft9), reported as a function of residue number. The rmsd values were computed for each couple of structures by using the program MOLMOL. Regions of cl-BABP/Gd-1 complex exhibiting rmsd larger than 3 Å from all the other analyzed structures are indicated in the plot in the left panel and mapped in pink on the protein structure in the right panel.

Intermolecular NOEs were obtained from a F_2-[^{15}N,^{13}C]-filtered-[^{1}H,^{1}H]-NOESY and a NOESY-[^{1}H,^{13}C]-HSQC spectra acquired at 600 MHz, as well as from a 3D F_1-[^{13}C]-filtered, F_2-[^{13}C]-separated, F_3-[^{15}N,^{13}C]-edited NOESY-HSQC spectrum acquired at 900 MHz. Mixing times of 80, 120, or 150 ms were used in all NOESY experiments. Finally, 2D [^{1}H,^{1}H]-ROESY experiments were performed with 50 and 90 ms spin-locking time. To obtain the maximum sensitivity, no filter was applied to this experiment. Pulse programs from the standard Bruker library were used.

Additional intermolecular restraints were derived from relaxation measurements on the adduct between a ^{15}N cl-BABP complexed with both the unlabeled diamagnetic Y-1 and paramagnetic Gd-1 in a P:Y-1:Gd-1 ratio of 1:4.5:0.5. In this way, it was possible to observe a fully saturated protein while keeping the concentration of the paramagnetic ligand sufficiently low, thereby avoiding bleaching out of amide signals. Amide proton longitudinal relaxation times were measured with an inversion recovery−HSQC sequence.[38] R_1 values were obtained by collecting a series of 10 spectra with delays between 0.08 and 3.48 s. The same experiments were repeated on a fully diamagnetic sample containing Y-1 with a P:L ratio of 1:5. Peak intensities were fitted to a monoexponential decaying function using three adjustable parameters within the program RELAXFIT.[44]

Protein Structure Calculation. Structure calculations were performed by simulated annealing in torsion angle space using the CYANA 2.1 package,[32] which implements an efficient protocol for structure calculation/automated NOE assignment.[45] The peak lists in CYANA format were generated by Format Converter.[46] The standard annealing protocol was used with 10000 steps of torsion angle dynamics; in each of the seven cycles, 100 structures were calculated and the 20 with the lowest target function were used in the next cycle. Then 150 NOEs were assigned manually and imposed in all stages of the protocol while all the other NOEs were automatically assigned, resulting in a total of 2187 upper distance bounds. Dihedral angle restraints were derived from TALOS.[47] In the last cycle, the 20 structures with the lowest target function were selected as the final bundle. The 10 best structures of the final bundle were used for the docking procedure.

Protein−Ligand Costructure Determination. The structure of the cl-BABP/Gd-1 adduct was obtained by data-driven docking using the software HADDOCK 2.0[48] in combination with CNS.[49] An ensemble of 10 NMR structures of the holo protein calculated by CYANA was used as input for the docking calculation. The starting coordinates of Gd-1 were obtained with the program SMILE.[50] The ligand molecule was built in complex with Yb(III), which is the metal ion most similar to Gd(III) in terms of atomic radius and mass among the ions currently defined in HADDOCK. A number of 11 freely rotatable dihedral angles were defined for the cholanoate and the linker moieties, while the DTPA residue was defined as rigid.

The definition of the "active and passive residues" was based on the experimental data collected as previously described,[21] including the chemical shift perturbations (CSPs) upon ligand binding and paramagnetic attenuation of amide resonances due to the presence of Gd(III). These data were used as ambiguous interaction restraints (AIR) to guide the docking. Unambiguous interaction restraints were further introduced in the calculations, including 14 intermolecular NOE-derived distances obtained from the analysis of the 3D edited/filtered NOESY, as well as 19 distances derived from paramagnetic relaxation enhancements. Paramagnetic contributions to longitudinal relaxation of amide protons, R_{1p}, were calculated as the difference in R_1 observed between the paramagnetic and the diamagnetic adduct and then converted into distance restraints according to the following equation:

$$R_{1p} = f \times K_{dip}/r^6 \quad (1)$$

where f is an occupancy factor and K_{dip} is the sum of the Solomon and Curie constants.[51] On the basis of estimates of the electronic relaxation times of the metal ion,[38] the lifetime of the protein−ligand adduct,[52] and the overall rotational correlation time,[25] a K_{dip} value of 2.3×10^7 s^{-1} Å^6, was determined. The occupancy factor was set to 0.1, corresponding to the paramagnetic/diamagnetic compound ratio in the sample. The errors in the relaxation rates were obtained from the fitting of the decay curves using a standard Monte Carlo approach. All the parameters used to estimate K_{dip} contain potential sources of error, but even a total uncertainty of 10% in the value of K_{dip} translates into less than 2% error in the calculated distance. However, instead of estimating the uncertainty in each distance, the approach taken was to assume that the errors from all sources can best be dealt with by adjusting the uncertainty through the distance bounds. On the basis of a number of structure calculation tests and evaluation of the penalty functions, the chosen bounds were ±2 Å.

The final upper distance limits used to calculate the holo protein structure in CYANA were used as unambiguous interaction restraints in order to ensure that the protein structure in the complex satisfied the experimentally derived intramolecular distances. Finally, TALOS restraints and hydrogen bond restraints derived from the CYANA structures were also used to calculate the structure of the complex by HADDOCK.

The HADDOCK docking protocol consists of three steps: (i) randomization of orientation and rigid body minimization, (ii) semirigid simulated annealing in torsion angle space, (iii) final refinement in Cartesian space with explicit solvent. The rigid body docking step was performed five times, with 1000 structures generated at each stage, the best 200 of which were refined in the semiflexible stage and subsequently in explicit water. Electrostatic and van der Waals terms were calculated with a 8.5 Å distance cutoff using the OPLS nonbonded parameters from the parallhdg5.3.pro parameter file.[53,54] Topology and parameters of the ligand were calculated using PRODRG server.[55] The dielectric constant ε was set to 10.0 and to 1.0 during explicit solvent refinement. The ligand was kept rigid during the semiflexible stage. The resulting solutions were clustered using the algorithm of Daura et al.[56] with 1 Å cutoff on the basis of the pairwise rmsd matrix for the carbon atoms of the ligand after fitting on the backbone atoms of the protein. The structures were divided in nine clusters ranked according to the HADDOCK score. We selected the best seven structures for every cluster and defined a final bundle of seven structures according to the HADDOCK score. The protein−ligand contacts were analyzed using the software LIGPLOT,[57] and the rmsd referred to ligand coordinates (carbons) was calculated after global superposition of protein backbone using the PROFIT program (Martin, A. C. R., Profit http://www.bioninf.org.uk/software/profit). The final ensemble of structures has been deposited in the PDB (2k62).

Acknowledgment. This research was supported by FIRB 2003 (grant RBNE03PX83_006) and by Cariverona Foundation. Consorzio Interuniversitario di Risonanze Magnetiche di Metalloproteine Paramagnetiche (CIRMMP) is gratefully acknowledged for measurements performed at 900 MHz. We are indebted to Alexandre Bonvin (Utrecht University) for helpful suggestions in the docking procedures and to Lucia Zetta for helpful suggestions. Clelia Cogliati is acknowledged for technical help in the assignment procedure.

References

(1) Kanematsu, M.; Kondo, H.; Goshima, S.; Kato, H.; Tsuge, U.; Hirose, Y.; Kim, M. J.; Moriyama, N. Imaging liver metastases: review and update. *Eur. J. Radiol.* **2006**, *58*, 217–228.

(2) Runge, V. M.; Pels Rijcken, T. H.; Davidoff, A.; Wells, J. W.; Stark, D. D. Contrast-enhanced MR imaging of the liver. *J. Magn. Reson. Imaging* **1994**, *4*, 281–289.

(3) Cabella, C.; Crich, S. G.; Corpillo, D.; Barge, A.; Ghirelli, C.; Bruno, E.; Lorusso, V.; Uggeri, F.; Aime, S. Cellular labeling with Gd(III) chelates: only high thermodynamic stabilities prevent the cells acting as "sponges" of Gd^{3+} ions. *Contrast Media Mol. Imaging* **2006**, *1*, 23–29.

(4) Vlasie, M. D.; Comuzzi, C.; van den Nieuwendijk, A. M.; Prudencio, M.; Overhand, M.; Ubbink, M. Long-range-distance NMR effects in a protein labeled with a lanthanide-DOTA chelate. *Chemistry* **2007**, *13*, 1715–1723.

(5) Chong, H. S.; Garmestani, K.; Bryant, L. H., Jr.; Milenic, D. E.; Overstreet, T.; Birch, N.; Le, T.; Brady, E. D.; Brechbiel, M. W. Synthesis and evaluation of novel macrocyclic and acyclic ligands as contrast enhancement agents for magnetic resonance imaging. *J. Med. Chem.* **2006**, *49*, 2055–2062.

(6) Anelli, P. L.; Lattuada, L.; Lorusso, V.; Lux, G.; Morisetti, A.; Morosini, P.; Serleti, M.; Uggeri, F. Conjugates of gadolinium complexes to bile acids as hepatocyte-directed contrast agents for magnetic resonance imaging. *J. Med. Chem.* **2004**, *47*, 3629–3641.

(7) Lu, Z. R.; Wang, X.; Parker, D. L.; Goodrich, K. C.; Buswell, H. R. Poly(L-glutamic acid) Gd(III)-DOTA conjugate with a degradable spacer for magnetic resonance imaging. *Bioconjugate Chem.* **2003**, *14*, 715–719.

(8) Curtet, C.; Maton, F.; Havet, T.; Slinkin, M.; Mishra, A.; Chatal, J. F.; Muller, R. N. Polylysine-Gd-DTPAn and polylysine-Gd-DOTAn coupled to anti-CEA F(ab′)2 fragments as potential immunocontrast agents. Relaxometry, biodistribution, and magnetic resonance imaging in nude mice grafted with human colorectal carcinoma. *Invest. Radiol.* **1998**, *33*, 752–761.

(9) Planchamp, C.; Montet, X.; Frossard, J. L.; Quadri, R.; Stieger, B.; Meier, P. J.; Ivancevic, M. K.; Vallee, J. P.; Terrier, F.; Pastor, C. M. Magnetic resonance imaging with hepatospecific contrast agents in cirrhotic rat livers. *Invest. Radiol.* **2005**, *40*, 187–194.

(10) Marinelli, E. R.; Neubeck, R.; Song, B.; Wagler, T.; Ranganathan, R. S.; Sukumaran, K.; Wedeking, P.; Nunn, A.; Runge, V.; Tweedle, M. Synthesis and evaluation of macrocyclic gadolinium chelates as hepatospecific MRI agents. *Acad. Radiol.* **2002**, *9* (1), S251–S254.

(11) Vander Elst, L.; Chapelle, F.; Laurent, S.; Muller, R. N. Stereospecific binding of MRI contrast agents to human serum albumin: the case of Gd-(S)-EOB-DTPA (Eovist) and its (*R*) isomer. *J. Biol. Inorg. Chem.* **2001**, *6*, 196–200.

(12) Pascolo, L.; Petrovic, S.; Cupelli, F.; Bruschi, C. V.; Anelli, P. L.; Lorusso, V.; Visigalli, M.; Uggeri, F.; Tiribelli, C. ABC protein transport of MRI contrast agents in canalicular rat liver plasma vesicles and yeast vacuoles. *Biochem. Biophys. Res. Commun.* **2001**, *282*, 60–66.

(13) Anelli, P. L.; Calabi, L.; de Haen, C.; Lattuada, L.; Lorusso, V.; Maiocchi, A.; Morosini, P.; Uggeri, F. Hepatocyte-directed MR contrast agents. Can we take advantage of bile acids? *Acta. Radiol. Suppl.* **1997**, *412*, 125–133.

(14) Uggeri, J.; Belletti, S.; Bussolati, O.; Dall'Asta, V.; Gazzola, G. C. Suppression of anionic amino acid transport impairs the maintenance of intracellular glutamate in Ha-ras-expressing cells. *Biochem. Biophys. Res. Commun.* **1995**, *211*, 878–884.

(15) Schmitt-Willich, H.; Brehm, M.; Ewers, C. L.; Michl, G.; Muller-Fahrnow, A.; Petrov, O.; Platzek, J.; Raduchel, B.; Sulzle, D. Synthesis and Physicochemical Characterization of a New Gadolinium Chelate: The Liver-Specific Magnetic Resonance Imaging Contrast Agent Gd-EOB-DTPA. *Inorg. Chem.* **1999**, *38*, 1134–1144.

(16) Hamm, B.; Staks, T.; Muhler, A.; Bollow, M.; Taupitz, M.; Frenzel, T.; Wolf, K. J.; Weinmann, H. J.; Lange, L. Phase I clinical evaluation of Gd-EOB-DTPA as a hepatobiliary MR contrast agent: safety, pharmacokinetics, and MR imaging. *Radiology* **1995**, *195*, 785–792.

(17) Pascolo, L.; Cupelli, F.; Anelli, P. L.; Lorusso, V.; Visigalli, M.; Uggeri, F.; Tiribelli, C. Molecular mechanisms for the hepatic uptake of magnetic resonance imaging contrast agents. *Biochem. Biophys. Res. Commun.* **1999**, *257*, 746–752.

(18) Brasch, R. C. New directions in the development of MR imaging contrast media. *Radiology* **1992**, *183*, 1–11.

(19) Dawson, P. A.; Oelkers, P. Bile acid transporters. *Curr. Opin. Lipidol.* **1995**, *6*, 109–114.

(20) von Dippe, P.; Levy, D. Reconstitution of the immunopurified 49 kDa sodium-dependent bile acid transport protein derived from hepatocyte sinusoidal plasma membranes. *J. Biol. Chem.* **1990**, *265*, 14812–14816.

(21) Assfalg, M.; Gianolio, E.; Zanzoni, S.; Tomaselli, S.; Russo, V. L.; Cabella, C.; Ragona, L.; Aime, S.; Molinari, H. NMR structural studies of the supramolecular adducts between a liver cytosolic bile acid binding protein and gadolinium(III)-chelates bearing bile acids residues: molecular determinants of the binding of a hepatospecific magnetic resonance imaging contrast agent. *J. Med. Chem.* **2007**, *50*, 5257–5268.

(22) Guariento, M.; Raimondo, D.; Assfalg, M.; Zanzoni, S.; Pesente, P.; Ragona, L.; Tramontano, A.; Molinari, H. Identification and functional characterization of the bile acid transport proteins in nonmammalian ileum and mammalian liver. *Proteins* **2008**, *70*, 462–472.

(23) Nichesola, D.; Perduca, M.; Capaldi, S.; Carrizo, M. E.; Righetti, P. G.; Monaco, H. L. Crystal structure of chicken liver basic fatty acid-binding protein complexed with cholic acid. *Biochemistry* **2004**, *43*, 14072–14079.

(24) Eliseo, T.; Ragona, L.; Catalano, M.; Assfalg, M.; Paci, M.; Zetta, L.; Molinari, H.; Cicero, D. O. Structural and dynamic determinants of ligand binding in the ternary complex of chicken liver bile acid binding protein with two bile salts revealed by NMR. *Biochemistry* **2007**, *46*, 12557–12567.

(25) Ragona, L.; Catalano, M.; Luppi, M.; Cicero, D.; Eliseo, T.; Foote, J.; Fogolari, F.; Zetta, L.; Molinari, H. NMR dynamic studies suggest that allosteric activation regulates ligand binding in chicken liver bile acid-binding protein. *J. Biol. Chem.* **2006**, *281*, 9697–9709.

(26) Tomaselli, S.; Ragona, L.; Zetta, L.; Assfalg, M.; Ferranti, P.; Longhi, R.; Bonvin, A. M.; Molinari, H. NMR-based modeling and binding studies of a ternary complex between chicken liver bile acid binding protein and bile acids. *Proteins* **2007**, *69*, 177–191.

(27) Shannon, R. D.; Previtt, C. T. Effective ionic radii in oxides and fluorides. *Acta Crystallogr., Sect. B: Struct. Sci.* **1969**, *25*, 925–946.

(28) Hsieh, W. Y.; Liu, S. Synthesis, characterization, and structures of indium In(DTPA-BA2) and yttrium Y(DTPA-BA2)(CH3OH) complexes (BA = benzylamine): models for 111In- and 90Y-labeled DTPA-biomolecule conjugates. *Inorg. Chem.* **2004**, *43*, 6006–6014.
(29) Kumar, K.; Chang, C. A.; Francesconi, L. C.; Dischino, D. D.; Malley, M. F.; Gougoutas, J. Z.; Tweedle, M. F. Synthesis, Stability, and Structure of Gadolinium(III) and Yttrium(III) Macrocyclic Poly(amino carboxylates). *Inorg. Chem.* **1994**, *33*, 3567–3575.
(30) Uggeri, F.; Aime, S.; Anelli, P. L.; Botta, M.; Brocchetta, M.; de Haeen, C.; Ermondi, G.; Grandi, M.; Paoli, P. Novel Contrast Agents for Magnetic Resonance Imaging. Synthesis and Characterization of the Ligand BOPTA and Its Ln(III) Complexes (Ln = Gd, La, Lu). X-ray Structure of Disodium (TPS-9-145337286-C-S)-[4-Carboxy-5,8,11-tris(carboxymethyl)-1-phenyl-2-oxa-5,8,11-triazatridecan-13-oato(5-)]gadolinate(2−) in a Mixture with Its Enantiomer. *Inorg. Chem.* **1995**, *34*, 633–643.
(31) Blomberg, N.; Sattler, M.; Nilges, M. 1H, 15N, and 13C resonance assignment of the PH domain from *C. elegans* UNC-89. *J. Biomol. NMR* **1999**, *15*, 269–70.
(32) Guntert, P. Automated NMR structure calculation with CYANA. *Methods Mol. Biol.* **2004**, *278*, 353–378.
(33) Kosen, P. A. Spin labeling of proteins. *Methods Enzymol.* **1989**, *177*, 86–121.
(34) Bertini, I.; Donaire, A.; Luchinat, C.; Rosato, A. Paramagnetic relaxation as a tool for solution structure determination: Clostridium pasteurianum ferredoxin as an example. *Proteins* **1997**, *29*, 348–358.
(35) Bertini, I.; Luchinat, C.; Rosato, A. The solution structure of paramagnetic metalloproteins. *Prog. Biophys. Mol. Biol.* **1996**, *66*, 43–80.
(36) Caravan, P.; Ellison, J. J.; McMurry, T. J.; Lauffer, R. B. Gadolinium(III) Chelates as MRI Contrast Agents: Structure, Dynamics, and Applications. *Chem. Rev.* **1999**, *99*, 2293–352.
(37) Aime, S.; Fasano, M.; Terreno, E. Lanthanide(III) chelates for NMR biomedical applications. *Chem. Soc. Rev.* **1998**, *27*, 19–29.
(38) Aime, S.; D'Amelio, N.; Fragai, M.; Lee, Y. M.; Luchinat, C.; Terreno, E.; Valensin, G. A paramagnetic probe to localize residues next to carboxylates on protein surfaces. *J. Biol. Inorg. Chem.* **2002**, *7*, 617–622.
(39) Assfalg, M.; Bertini, I.; Del Conte, R.; Giachetti, A.; Turano, P. Cytochrome c and organic molecules: solution structure of the *p*-aminophenol adduct. *Biochemistry* **2007**, *46*, 6232–6238.
(40) Benazeth, S.; Purans, J.; Chalbot, M. C.; Nguyen-Van-Duong, M. K.; Nicolas, L.; Keller, F.; Gaudemer, A. Temperature and pH Dependence XAFS Study of Gd(DOTA)(−) and Gd(DTPA)(2)(−) Complexes: Solid State and Solution Structures. *Inorg. Chem.* **1998**, *37*, 3667–3674.
(41) Ragona, L.; Colombo, G.; Catalano, M.; Molinari, H. Determinants of protein stability and folding: comparative analysis of beta-lactoglobulins and liver basic fatty acid binding protein. *Proteins* **2005**, *61*, 366–376.
(42) Delaglio, F.; Grzesiek, S.; Vuister, G. W.; Zhu, G.; Pfeifer, J.; Bax, A. NMRPipe: a multidimensional spectral processing system based on UNIX pipes. *J. Biomol. NMR* **1995**, *6*, 277–293.
(43) Johnson, B. A. Using NMRView to visualize and analyze the NMR spectra of macromolecules. *Methods Mol. Biol.* **2004**, *278*, 313–352.
(44) Fushman, D.; Cahill, S.; Cowburn, D. The main-chain dynamics of the dynamin pleckstrin homology (PH) domain in solution: analysis of 15N relaxation with monomer/dimer equilibration. *J. Mol. Biol.* **1997**, *266*, 173–194.
(45) Herrmann, T.; Guntert, P.; Wuthrich, K. Protein NMR structure determination with automated NOE assignment using the new software CANDID and the torsion angle dynamics algorithm DYANA. *J. Mol. Biol.* **2002**, *319*, 209–227.
(46) Fogh, R.; Ionides, J.; Ulrich, E.; Boucher, W.; Vranken, W.; Linge, J. P.; Habeck, M.; Rieping, W.; Bhat, T. N.; Westbrook, J.; Henrick, K.; Gilliland, G.; Berman, H.; Thornton, J.; Nilges, M.; Markley, J.; Laue, E. The CCPN project: an interim report on a data model for the NMR community. *Nat. Struct. Biol.* **2002**, *9*, 416–418.
(47) Cornilescu, G.; Delaglio, F.; Bax, A. Protein backbone angle restraints from searching a database for chemical shift and sequence homology. *J. Biomol. NMR* **1999**, *13*, 289–302.
(48) Dominguez, C.; Boelens, R.; Bonvin, A. M. HADDOCK: a protein−protein docking approach based on biochemical or biophysical information. *J. Am. Chem. Soc.* **2003**, *125*, 1731–1737.
(49) Brunger, A. T.; Adams, P. D.; Clore, G. M.; DeLano, W. L.; Gros, P.; Grosse-Kunstleve, R. W.; Jiang, J. S.; Kuszewski, J.; Nilges, M.; Pannu, N. S.; Read, R. J.; Rice, L. M.; Simonson, T.; Warren, G. L. Crystallography & NMR system: A new software suite for macromolecular structure determination. *Acta Crystallogr., Sect. D: Biol. Crystallogr.* **1998**, *54*, 905–921.
(50) Eufri, D.; Sironi, A. SMILE—shaded molecular imaging on low-cost equipment. *J. Mol. Graph.* **1989**, *7*, 165–169, 158.
(51) Bertini, I.; Luchinat, C. NMR of paramagnetic substances. *Coord. Chem. Rev.* **1996**, *150*, 1–296.
(52) Ayers, S. D.; Nedrow, K. L.; Gillilan, R. E.; Noy, N. Continuous nucleocytoplasmic shuttling underlies transcriptional activation of PPARgamma by FABP4. *Biochemistry* **2007**, *46*, 6744–6752.
(53) Jorgensen, W. L.; Tirado-Rives, J. The OPLS (optimized potentials for liquid simulations) potential functions for proteins, energy minimizations for crystals of cyclic peptides and crambin. *J. Am. Chem. Soc.* **1988**, *110*, 1657–1666.
(54) Linge, J. P.; Williams, M. A.; Spronk, C. A.; Bonvin, A. M.; Nilges, M. Refinement of protein structures in explicit solvent. *Proteins* **2003**, *50*, 496–506.
(55) van Aalten, D. M.; Bywater, R.; Findlay, J. B.; Hendlich, M.; Hooft, R. W.; Vriend, G. PRODRG, a program for generating molecular topologies and unique molecular descriptors from coordinates of small molecules. *J. Comput.-Aided Mol. Des.* **1996**, *10*, 255–262.
(56) Daura, X.; Gademan, K.; Jaun, B.; Seebach, D.; van Gunsteren, W. F.; Mark, A. Peptide folding: when simulation meets experiment. *Angew. Chem., Int. Ed.* **1999**, *38*, 236–240.
(57) Wallace, A. C.; Laskowski, R. A.; Thornton, J. M. LIGPLOT: a program to generate schematic diagrams of protein−ligand interactions. *Protein Eng.* **1995**, *8*, 127–134.

JM800820B